ELSEVIER

Journal of Molecular Catalysis A: Chemical 121 (1997) 157–169

JOURNAL OF MOLECULAR CATALYSIS A: CHEMICAL

Conversion of 2-octanol over nickel–alumina, cobalt–alumina, and alumina catalysts

Sivaraj Chokkaram, Ram Srinivasan, Diane R. Milburn, Burtron H. Davis *

Center for Applied Energy Research, 3572 Iron Works Pike, Lexington, KY 40511, USA

Received 22 April 1996; accepted 31 December 1996

Abstract

Structural characterization of Co–Al and Ni–Al coprecipitated catalysts has been accomplished using techniques such as X-ray diffraction, DTA, TGA, TG-MS, BET surface area and pore volume. The catalyst samples were prepared by coprecipitation of cobalt (or nickel) and aluminum from their aqueous salt solutions. The interaction of Co (or Ni) with aluminum has been investigated by X-ray diffraction as a function of calcination temperature. The results indicate that the interaction between Co and Al can lead to the formation of a normal spinel of $CoAl_2O_4$ at a very low temperature such as 473 K. On the other hand the interaction between Ni and Al is not sufficient to form well crystallized $NiAl_2O_4$ species at low temperatures but nickel–aluminate formation was seen above 973 K. The activity and selectivity of these catalysts for 2-octanol conversion are dependent on the reaction temperature, liquid hour space velocity (LHSV) as well as on the calcination temperature. The dehydrogenation activity of nickel based catalysts is attributed to the presence of nickel oxide whereas the dehydration activity is due to the spinel phase. The differences in the dehydration activity between alumina and nickel–alumina is mostly because of the incomplete formation of spinel phase (i.e., low temperature calcined samples). Catalytic activity of cobalt–alumina catalysts is comparable with that of alumina catalysts towards 2-octanol conversion.

Keywords: Octanol conversion; Nickel–alumina; Cobalt–alumina; Catalyst characterization (XRD/DTA/TGA/TG-MS/BET); Calcination; Dehydrogenation; Dehydration

1. Introduction

Supported metal oxide catalysts attract much attention because of their wide application in a variety of industrially important reactions. The nature and extent of interaction between the support material and the dispersed metal oxide species are widely studied. These may depend upon the method of preparation, concentration of metal species in the catalyst, nature of the support, calcination temperature, and duration of calcination [1–9]. Although supported metal oxide systems have been the subject of numerous investigations, the nature of the interaction between the support and metal species in many systems is still not understood clearly. At one extreme of metal support interactions, interoxidic spinel compounds may be formed. The ideal spinel structure consists of a cubic close-packed array of anions, with one eighth of the tetrahedral and one half of the octahedral interstices occupied by cations, so that the cation to anion ratio is 3:4. In a binary oxide spinel [8], AB_2O_4,

* Corresponding author.

PII S1381-1169(97)00018-6

two extreme distributions of cations among the available tetrahedral and octahedral sites are possible (the ions in parentheses occupy octahedral sites): the 'normal' distribution with $A(B_2)O_4$ and the 'inverse' distribution with $B(AB)O_4$.

In normal bimetallic spinels (i.e., $CoAl_2O_4$), the Al^{3+} ions are located in octahedral sites and they are considered to have weak acidity [1]. On the other hand, in inverse bimetallic spinels (i.e., $NiAl_2O_4$) the Al^{3+} ions are expected to be in tetrahedral coordination sites and they are expected to exhibit significant acidic character [1].

Several surface models concerning the interaction between a metal oxide and γ-alumina have been proposed in literature. The model proposed by Hercules et al. [3] for γ-alumina supported nickel oxide allows Ni^{2+} ions to diffuse into the surface lattice vacancies of the alumina spinel structure.

A major interest in Co/Al_2O_3 catalysts has centered on interactions between the metal and support. It is known that metal–support interactions may appreciably affect the surface properties of these catalysts, and hence their reactivities. The migration of metal ions into the alumina matrix is a common phenomenon in metal supported catalysts and it has been reported that the migration process may be limited to the first few layers of the support [9]. It has been reported that in Co/Al_2O_3 catalysts the surface consists of dispersed $CoAl_2O_4$ spinel at low loading while at higher loading, crystallite Co_3O_4 is also present. Arnoldy and Mouljin [9] have identified, through TPR studies, a number of phases that are present in these catalysts.

Recently Murthy and Swamy [7] reported the synthesis and characterization of coprecipitated Co–Al mixed oxide catalysts. According to these authors the stoichiometry of the mixed oxide can be represented as $Co_{(1+x)}Al_{(2-x)}O_4$ (where $x = 0$ to 1). According to Murthy and Swamy [7] the activity for the dehydration of 2-propanol is predominant at $x = 0$ and for the dehydrogenation reaction at $x = 1$. The authors also indicated that the dehydration activity for 2-propanol resides predominantly with the Al^{3+} ions located in the tetrahedral coordination sites of the spinel and that the dehydrogenation activity results from Co^{3+} sites located in the octahedral coordination sites of the spinel.

In alumina, the Al^{3+} occupies both the tetrahedral and octahedral sites. It is possible for the two sites to have different catalytic properties for alcohol dehydration, both with respect to activity and selectivity. If this is the case, the normal spinel (i.e., cobalt–aluminate) and inverse spinel (i.e., nickel–aluminate) are expected to have different catalytic properties. Thus, the present study with the normal and inverse spinels was conducted to learn whether this was the case.

2. Experimental

2.1. Catalyst preparation

Cobalt and nickel aluminate samples were prepared by a coprecipitation method. In a typical experiment Al and Co (or Ni) are coprecipitated from an aqueous nitrate solution by adding an aqueous ammonium carbonate (1 M) solution to produce a pH of about 8. The molar ratio of Al/Co and Al/Ni in the solution for this study was 2.0. The precipitates were collected by filtration, washed and dried at 373 K for 20 h. Portions of the catalyst samples were calcined for 4 h in air at temperatures ranging from 473 to 1173 K.

Alumina was prepared from an aqueous aluminium nitrate solution following an experimental procedure similar to that used for the cobalt or nickel containing alumina catalysts. Portions of the alumina were calcined for 4 h in air at temperatures ranging from 473 to 1173 K.

2.2. Catalyst characterization

Nitrogen adsorption measurements at 77 K were carried out using a Quantachrome Au-

tosorb 6 instrument. The surface area was calculated using the BET equation [10] and the nitrogen adsorption data. The pore volume was calculated from desorption data assuming a cylindrical pore shape with refinements developed by Broekhoff and deBoer [11] which correct for the adsorbed layer of nitrogen.

X-ray diffraction measurements were carried out using a Philips X-ray diffractometer operating at 25 kV, 20 mA, and CuK_α radiation ($\lambda = 0.15418$ nm). The crystal phases of the sample were identified by overlaying the standard ASTM diffraction pattern of an expected compound; a match was based both upon peak position and relative intensity. This process was repeated with several expected compounds which allowed an identification of the various phases present in the sample.

Differential thermal analysis (DTA) and thermogravimetric analysis (TGA) of Co and Ni alumina precursors were conducted simultaneously using a Seiko TGA/DTA 320 instrument which is coupled to a VG Micromass quadrupole mass spectrometer. The experiments, unless noted otherwise, were conducted using a helium purge gas (100 mL/min) at a heating rate of 10 K/min. Platinum crucibles were used in all cases, and α-Al_2O_3 was used as a reference material. The mass spectrometer was used to conduct 'evolved gas analysis' (EGA) concurrently with the simultaneous DTA/TG experiments.

2.3. Catalytic activity measurements

In a typical experiment to measure catalytic activity, about 0.5 g (the actual amount was determined for each run) of the sample was diluted with 0.5 g of glass beads (80–100 mesh) and loaded into a tubular, fixed bed reactor where it was held between two quartz wool plugs. A chromel–alumel thermocouple is located near the catalyst bed to monitor the reaction temperature, and to control the temperature. The catalyst was pretreated at 573 K in nitrogen flow for 5 h prior to the reaction. 2-octanol was pumped over the catalyst and the products were collected at intervals during a 6–8 h test period. The liquid hour space velocity (LHSV) of 2-octanol was varied from 0.81 to 15 cc/h. Products were analyzed by gas chromatograph using a DB5 capillary column.

3. Results and discussion

The effect of calcination temperature on the structural and catalytic properties of cobalt–alumina, nickel–alumina, and alumina catalysts was measured. The data to show the effect of calcination temperature on the BET surface area, pore volume, crystal structure and crystallite size of the coprecipitated Co–Al and Ni–Al catalysts are summarized in Tables 1 and 2. The BET areas of Ni–Al samples decrease from 127 to 94 m^2/g as the calcination temperature in-

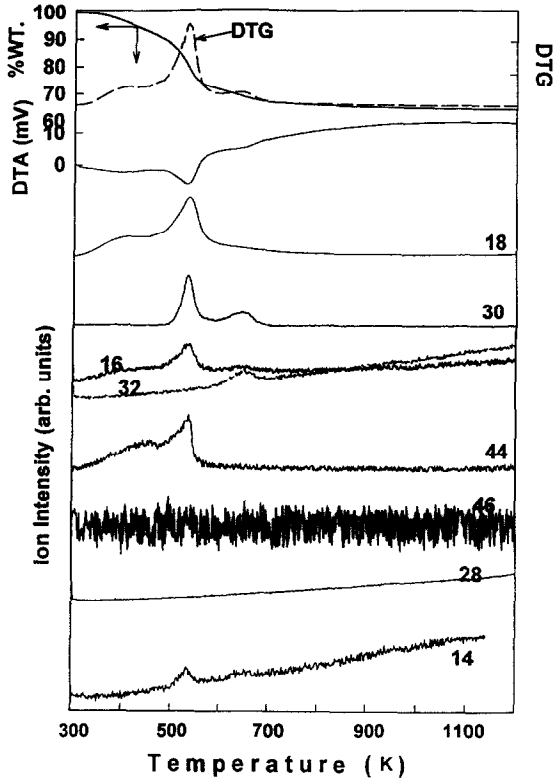

Fig. 1. DTA, DTG and TG/MS results of cobalt–alumina coprecipitated catalyst precursor.

Table 1
Effect of calcination on the surface area, pore volume and crystal structure of cobalt–alumina coprecipitated catalyst

Calcination temperature (K)	BET surface area (m^2/g)	Pore volume (cc/g)	XRD phases	Crystallite sizes [a] (Å)
473	156	0.30	$CoAl_2O_4$ and traces of Co_2O_3	71 (311)
				81 (440)
673	198	0.37	$CoAl_2O_4$ and traces of Co_2O_3	83 (220)
				93 (311)
				86 (440)
773	169	0.37	$CoAl_2O_4$	103 (220)
				105 (311)
				89 (440)
973	116	0.39	$CoAl_2O_4$	130 (220)
				131 (311)
				128 (440)
1173	79	0.36	$CoAl_2O_4$	229 (220)
				209 (311)
				210 (440)

[a] Crystallite sizes were calculated using X-ray line broadening technique.

creases from 673 to 1173 K. Similarly the BET surface areas for coprecipitated Co–Al catalysts decrease from 156 to 79 m^2/g as the calcination temperature increases from 473 to 1173 K. The pore volume does not depend on the calcination temperature.

DTA, DTG and TG-MS results for Co-containing catalyst precursor show an endothermic peak centered at about 538 K (Fig. 1). The DTG results show that the dominant weight loss occurs at temperatures between 468 and 538 K. The experimental weight loss obtained from TG data for cobalt–alumina was in the range of 31 wt% and the theoretical weight loss for this sample, assuming it to be $Al(OH)_3$ and $Co(OH)_2$, is 29.4%. Below 468 K, a gradual loss of weight, and the evolution of both H_2O and CO_2, is observed in Fig. 1. The endotherm and a maximum in the derivation of the weight loss are centered at about 540 K and correspond

Table 2
Effect of calcination temperature on the surface area, pore volume and crystal structure of nickel–alumina coprecipitated catalyst

Calcination temperature (K)	BET surface area (m^2/g)	Pore volume (cc/g)	XRD phases	$NiAl_2O_4$ crystallite sizes [a] (Å)
473	—	—	poorly crystalline NiO and $NiAl_2O_4$	< 25
673	127	0.20	poorly crystalline NiO and $NiAl_2O_4$	< 25
773	115	0.21	poorly crystalline NiO and $NiAl_2O_4$	< 25
873	—	—	poorly crystalline NiO and $NiAl_2O_4$	< 28
973	105	0.19	NiO and $NiAl_2O_4$	32 (400)
				34 (311)
				28 (440)
1073	—	—	NiO and $NiAl_2O_4$	47 (400)
				63 (311)
				63 (440)
1173	94	0.21	NiO and $NiAl_2O_4$	79 (400)
				86 (311)
				95 (440)

[a] Crystallite sizes were calculated using X-ray line broadening technique.

to the evolution of water (mass 18) and CO_2 (mass 44) (Fig. 1). During the endotherm at 540 K, NO (mass 30) is also evolved, and this indicates that the washing did not remove all of the nitrate. Likewise, the evolution of CO_2 indicates that some CO_3^{2-} (or HCO_3^{2-}) remained with the catalyst. However, the mass spectroscopic data is qualitative so that a measure of the impurity nitrate and carbonate is not possible. The small endotherm centered at about 650 K, and a small weight loss with the observation of NO evolution, likely corresponds to a crystallization. These events will occur at a higher temperature when the sample is heated at 20°/min than when it is heated for 4 h at a given temperature during the calcination procedure; hence, the temperatures shown for the TGA data (Figs. 1 and 2) and the XRD traces (Figs. 3 and 4) cannot be compared directly. The decomposition of a salt with evolution of gas is usually an endothermic event whereas the crystallization with loss of surface area is exothermic. Thus, whether the observed heat change is endothermic or exothermic will depend upon the balance of these two, or more, events (e.g. [12]). In any event, the evolution of gas combined with the weight loss clearly indicate that the endothermic peak centered at 540 K is the result of a decomposition reaction.

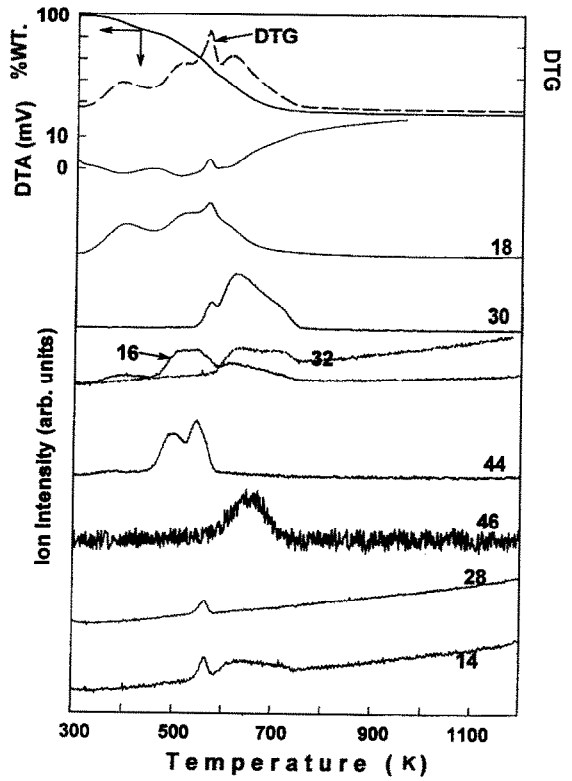

Fig. 2. DTA, DTG and TG/MS results of nickel–alumina coprecipitated catalyst precursor.

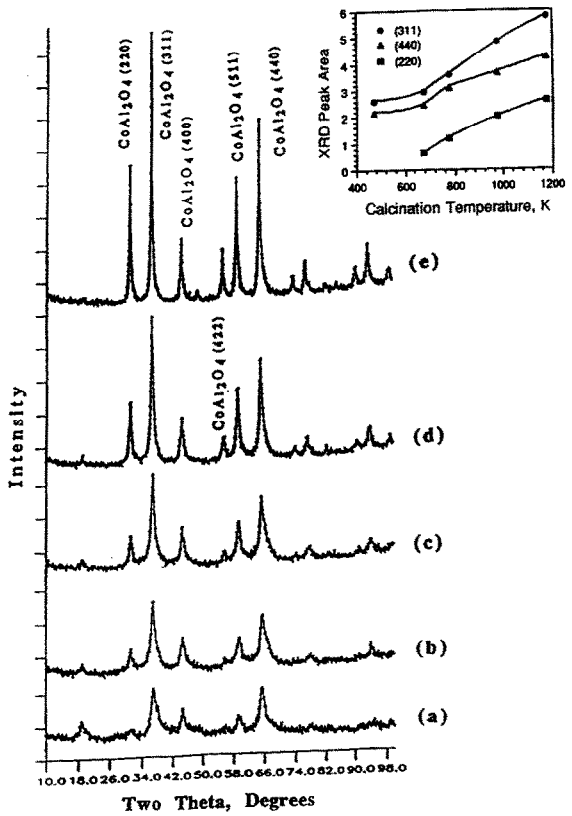

Fig. 3. Effect of calcination temperature on the crystallinity of cobalt–alumina coprecipitated mixed oxide catalyst. (a) 573 K, (b) 673 K, (c) 773 K, (d) 973 K, (e) 1173 K.

The DTA and TG results for nickel–alumina samples show a series of peaks centered at about 390, 550 and 590 K; however, these peaks are superimposed upon a broad endotherm background. For example, water is lost during a temperature range of about 300–700 K; the rate of maximum water evolution, based on the M.S. data, correspond to the three peaks centered at 390, 550 and 590 K. The loss of CO_2 becomes noticeable at about 450 K, and

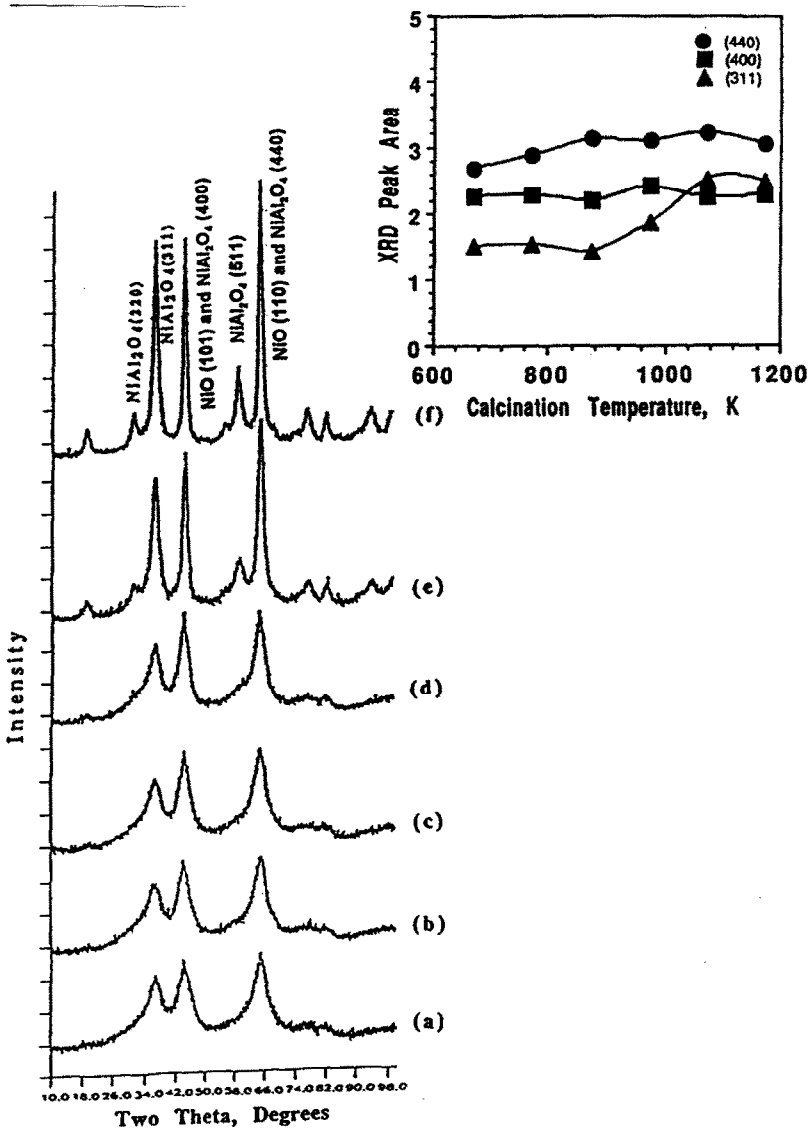

Fig. 4. Effect of calcination temperature on the crystallinity of nickel–alumina coprecipitated mixed oxide catalysts. (a) 673 K, (b) 773 K, (c) 873 K, (d) 973 K, (e) 1073 K, (f) 1173 K.

attains a maximum at about 500 and 540 K. The loss of NO attains a maximum rate that corresponds to the 590 K exotherm; this rate is superimposed upon a broad NO loss curve that is centered at about 635 K. The loss of NO_2 (mass 46) follows rather closely the second, broad evolution peak for NO. The combination of NO_2 with H_2O will impact the appearance of NO_2 in the M.S. The experimental weight loss for the nickel–aluminum sample is about 42 wt% whereas the theoretical value would be 29% for the decomposition of the nickel–aluminum hydroxides. Thus, it appears that the nickel–aluminum containing solid contains more nitrate and carbonate than the corresponding cobalt–aluminum solid.

The XRD results for the cobalt–alumina catalysts show the presence of a $CoAl_2O_4$ phase at calcination temperatures ranging from 473 to 1173 K (Fig. 3). The 2θ values (and lattice plane) corresponding to the major peaks are 31.4 (220), 37 (311) and 65.4 (440) and these

match closely with the standard $CoAl_2O_4$ phase (ASTM #10-458). The ASTM standard data for cobalt aluminate show that the 311 plane is the most intense ($I = 100$) followed by 220 ($I = 65$) and 440 ($I = 40$) planes. Present experimental results also show that the 311 plane is the most intense ($I = 100$) followed by 440 ($I = 74$ to 83) and 220 ($I = 21$ to 46) planes. The areas (intensities) of the XRD peaks corresponding to the $CoAl_2O_4$ phase increase (inset of Fig. 3) with increasing calcination temperature. The crystallite sizes calculated from XRD line-broadening of the cobalt–alumina samples increase (Table 1) from about 7 to 23 nm as the calcination temperature increases from 473 to 1173 K. The XRD peak areas and crystallite sizes of cobalt–alumina samples show that both the $CoAl_2O_4$ phase content and its crystallite size increase with the calcination temperature. The XRD results also show that the coprecipitation method leads initially (473 K calcination) to the formation of trace quantities of Co_2O_3 and Co_3O_4 in addition to $CoAl_2O_4$ phase (major). As the calcination temperature increases, the quantity of the $CoAl_2O_4$ phase increases. Chin and Hercules [13] reported the initial formation of Co_3O_4 during the calcination of an impregnated Co/Al_2O_3 catalyst.

X-ray diffraction patterns of nickel–alumina samples show that at low calcination temperatures (Fig. 4) the XRD peaks are broad and these peaks become sharper with an increase in the calcination temperature. The 2θ values, corresponding to the three major peaks at $2\theta = 37$ (311), 45 (400), and 65.6 (440) closely match those expected for the $NiAl_2O_4$ (ASTM #10-339) phase. However, the relative intensities of these peaks do not match exactly the ASTM standard. For example, the ASTM standard data of nickel–aluminate show that the 311 plane is the most intense ($I = 100$) followed by 400 plane ($I = 65$) and 440 plane ($I = 60$). However, for the present results, the 440 plane is the most intense ($I = 100$) followed by the 400 plane ($I = 71$ to 84) and the 311 plane ($I = 46$ to 81). The discrepancies in the relative intensities of these peaks may be due to the presence of impurities, such as nickel oxide, and/or preferred growth in certain crystal directions. The XRD patterns of nickel–alumina samples from the present study do not show well defined peaks corresponding to the nickel oxide phase. The area under the XRD peak is often considered to represent the integrated intensity of the peak. For most of the metal oxides the integrated intensity of a particular XRD peak is proportional to the amount of phase corresponding to that peak. The XRD results from the present study show that the areas under the three major peaks (corresponding to 311, 400 and 440 planes) remain almost constant throughout the calcination temperature range of 673 to 1173 K (inset of Fig. 4). These results clearly show that the nickel–alumina samples contain almost equal amount of nickel–aluminate phase irrespective of their calcination temperature; they differ only with respect to crystallinity. This is further illustrated by the crystallite size which increases from 2.5 to 9.5 nm as the calcination temperature increases from 473 to 1173 K (Table 2). The crystallite sizes obtained from this study (from the X-ray diffraction pattern (Fig. 3) and crystallite size data (Table 2)) are inconsistent with the results reported by Lansink et al. [14]. The $NiAl_2O_4$ particles obtained below 973 K calcination temperatures in the present study are considerably smaller than reported by Lansink et al. [14].

The XRD pattern for the dried nickel–aluminum containing material has three very broad and low intensity peaks that have 2θ values in the regions of the three major peaks for $NiAl_2O_4$; however, the peak maxima positions do not have the exact 2θ values for $NiAl_2O_4$. The XRD pattern for the cobalt–aluminum material exhibits low intensity, broad peaks that could be due to very small crystalline $CoAl_2O_4$. Superimposed upon these broad peaks are a few sharp low intensity peaks that we have not been able to identify using the ASTM reference data.

The specific surface area of a cube or sphere

is related [15,16] to the edge or diameter of the particle by the equation $S = (6/\rho D)(1/F)$ where S is the surface area, ρ is the density, D is the edge or diameter, and $1/F$ is the packing factor [15] to correct for surface contact points that are unavailable for nitrogen adsorption. The log(surface area, m^2/g) versus log(crystallite, nm) plots (Fig. 5) for Co–Al and Ni–Al samples yield packing factor ($1/F$) values of 0.70 and 0.25, respectively. The assumption made by Allred et al. [15] for the correction of unavailable surface area is based on spherical particles. Deviations in the experimentally determined packing factor values can be associated with the irregular shape of particles. In the present study of cobalt–alumina and nickel–alumina systems, the packing factor value for cobalt–alumina samples is near to the one usually observed (i.e., 0.7) but the packing factor is far from unity (i.e., 0.25) for nickel–alumina material. These results suggest that the nickel–alumina particles may be very irregular in shape. Analysis of the nickel–alumina sample (calcined at 1173 K) by SEM-EDAX showed that the particles are irregular in shape, and have an Al/Ni ratio approximately 2.0, as expected, and at the resolution of the instrument, have a uniform distribution of Ni and Al.

Alcohol conversion provides a dehydration/dehydrogenation selectivity, alkene

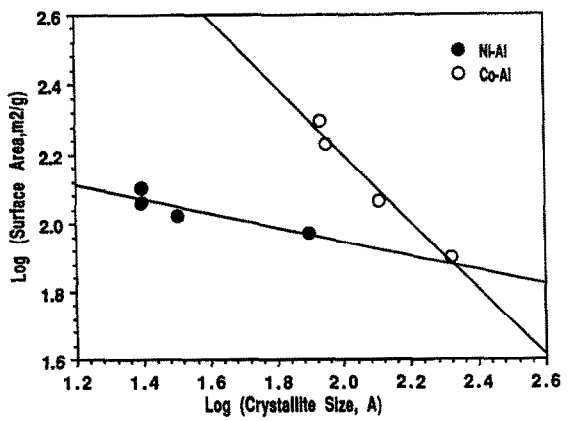

Fig. 5. Crystallite size–surface area relationship for (●) nickel–alumina and (○) cobalt–alumina coprecipitated catalysts calcined at temperatures ranging from 473 to 1173 K.

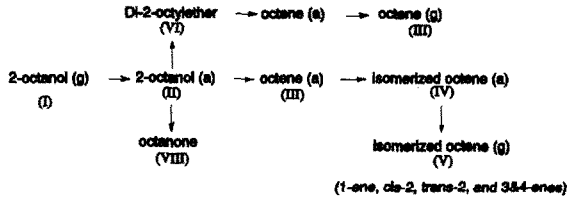

Scheme 1.

selectivities, and an ether selectivity. Thus, the conversion of 2-octanol may occur through (e.g., [17–20]) several sequence of reactions such as shown in Scheme 1, where (a) refers to the adsorbed phase and (g) to the gas phase. The selectivity for one of the product(s), X_i, is denoted as S_{X_i} (where X_i stands for dehydration products (III + VI), octenes (III), ethers (VI) and dehydrogenation (VIII) product) which is defined as:

$$S_{X_i} = \frac{\text{amount of } X_i \text{ formed} \times 100}{\text{conversion of 2-octanol.}}$$

Similarly, the octene distribution, which represents the selectivity for one octene among the octene products, is defined as

$$S' = \frac{(\text{amount of one of the octene formed} \times 100)}{\text{total octenes formed.}}$$

Results for the conversion of 2-octanol over alumina, cobalt–alumina, and nickel–alumina catalysts are presented in Tables 3–7. The selectivity for dehydrogenation, dehydration, and isomerization depend on the type of catalyst, LHSV, catalyst calcination temperature and the reaction temperature. The selectivities for 1-octene, *cis*-2-octene, and *trans*-2-octene among the octenes (Tables 3–6) depend mostly on the type of catalyst, LHSV and reaction temperature.

The data for 2-octanol conversion over alumina, cobalt–alumina and nickel–alumina catalysts show a linear relationship between conversion and the reciprocal LHSV (Figs. 6 and 7) up to conversions of about 50%. Thus, the 2-octanol conversion over these catalysts follows zero order kinetics in the conversion range of 0 to 50% but, at higher conversions, there is a

Table 3
Conversion of 2-octanol over alumina calcined at 673 K in air (alumina is obtained from aluminum nitrate aqueous solution by precipitation)

Reaction temperature (K)	LHSV [a]	Conversion [b] (mol%)	Distribution of octenes (mol%)				Selectivity for octanone [c]	Selectivity for ethers [c]
			1-	*c*-2-	*t*-2-	3- and 4-		
493	2.5	13.2	47.0	42.5	10.3	0.2	tr	17.4
503	2.5	19.2	44.0	44.4	11.7	0.1	tr	15.6
513	2.5	30.6	40.9	45.0	14.0	0.1	tr	12.4
523	2.5	58.9	38.7	46.2	14.8	0.3	tr	7.3
543	2.5	95.3	35.0	47.1	17.5	0.4	tr	0.7
553	2.5	97.4	33.2	47.5	18.6	0.7	tr	0.2
523	2.5	58.9	42.0	45.3	12.6	0.1	0.3	11.0
523	4.1	45.6	42.9	45.0	12.0	0.1	0.5	11.0
523	6.5	36.8	43.4	44.7	11.8	0.1	0.3	12.3
523	9.7	28.3	44.3	44.3	11.3	0.1	0.3	12.0
523	15.0	17.5	44.6	44.0	11.3	0.1	0.4	12.3
523	19.2	10.0	44.8	43.8	11.3	0.1	0.3	12.0

[a] Liquid hourly space velocity (cc/h/g catalyst).
[b] Conversion is given for octenes, octanone, dioctylethers and other products.
[c] Selectivity is equal to the amount of product formed divided by total octanol converted.

departure from zero order kinetics (Figs. 6 and 7), as has been reported for alumina (e.g., [21]).

The temperature dependency of 2-octanol over alumina, nickel–alumina and cobalt–alumina is shown in Fig. 8 in the form of Arrhenius plots (ln(conversion) versus $1/T$). The data were well fitted with a regression coefficient of above 0.95. The activation energies (Table 7) calculated from these Arrhenius plots (Fig. 8) vary from 16 to 31 kcal/mol for the conversion of 2-octanol, 17–31 kcal/mol for the dehydration of 2-octanol and 10–25 kcal/mol for the dehydration of 2-octanol to ethers ($T = 493$–533 K). The activation energy values obtained in the present study are consistent with the results reported for earlier studies [20,22–24]. For example, an activation energy value of 32.2 kcal/mol was reported for the dehydration of 2-octanol over yttria catalysts in the reaction temperature range of 513 to 618 K [22]. Similarly Narayanan et al. [24] reported the activation values in the range of 25 to 33.4

Table 4
Conversion of 2-octanol over alumina calcined at 1173 K in air (alumina is obtained from aluminum nitrate aqueous solution by precipitation)

Reaction temperature (K)	LHSV [a]	Conversion [b] (mol%)	Distribution of octenes (mol%)				Selectivity for octanone [c]	Selectivity for ethers [c]
			1-	*c*-2-	*t*-2-	3- and 4-		
493	2.5	22.6	47.0	43.5	9.4	0.1	1.5	11.8
503	2.5	34.2	44.5	45.2	10.2	0.1	0.8	10.5
508	2.5	43.6	43.5	45.2	10.6	0.1	0.4	9.3
523	2.5	89.7	34.4	47.7	17.3	0.6	tr	0.7
523	6.5	59.9	37.9	46.8	15.0	0.3	tr	3.7
523	9.7	43.8	39.2	46.3	14.3	0.2	tr	4.3
523	15.0	33.0	40.4	45.7	13.7	0.2	tr	4.6
523	19.2	27.6	40.8	45.3	13.6	0.3	tr	4.2

[a] Liquid hourly space velocity (cc/h/g catalyst).
[b] Conversion is given for octenes, octanone, dioctylethers and other products.
[c] Selectivity is equal to the amount of product formed divided by total octanol converted.

Table 5
Conversion of 2-octanol over nickel–alumina coprecipitated catalysts

Reaction temperature (K)	LHSV [a]	Conversion [b] (mol%)	Distribution of octenes (mol%)				Selectivity for octanone [c]	Selectivity for ethers [c]
			1-	*c*-2-	*t*-2-	3- and 4-		
NiAl-673								
493	0.8	5.8	51.0	38.2	10.6	0.2	67.2	5.2
513	0.8	12.2	47.0	41.8	11.0	0.2	33.6	9.0
553	0.8	52.6	38.7	44.7	16.0	0.6	18.8	4.9
523	1.2	21.3	47.1	40.7	11.8	0.4	42.5	5.3
523	1.7	16.0	46.9	41.2	11.7	0.2	40.6	5.6
523	2.5	12.1	47.7	40.8	11.4	0.1	38.3	5.1
523	4.1	7.9	48.3	40.3	11.2	0.2	38.5	5.1
523	6.5	5.1	48.4	40.3	11.1	0.2	40.5	4.9
NiAl-1173								
493	0.8	4.4	51.8	38.0	10.0	0.2	30.9	4.5
513	0.8	17.5	47.3	42.0	10.6	0.1	23.7	6.3
533	0.8	48.0	42.2	45.9	11.5	0.4	18.5	5.0
523	1.7	30.8	44.5	43.3	11.3	0.9	23.3	4.1
523	2.5	23.2	46.0	43.1	10.2	0.7	21.6	4.0
523	4.1	15.7	46.2	43.3	10.1	0.4	22.9	6.0

[a] Liquid hourly space velocity (cc/h/catalyst).
[b] Conversion is given for octenes, octanone, dioctylethers and other products.
[c] Selectivity is equal to the amount of product formed divided by total octanol converted.

Table 6
Conversion of 2-octanol over cobalt–alumina coprecipitated catalysts

Reaction temperature (K)	LHSV [a]	Conversion [b] (mol%)	Distribution of octenes (mol%)				Selectivity for octanone [c]	Selectivity for ethers [c]
			1-	*c*-2-	*t*-2-	3- and 4-		
CoAl-673								
493	2.5	7.7	51.6	39.1	9.3	—	5.6	11.4
503	2.5	13.3	49.9	40.6	9.4	0.1	3.9	11.5
508	2.5	16.8	48.9	41.4	9.7	—	3.5	10.6
513	2.5	21.6	47.8	42.2	9.9	0.1	3.1	11.5
523	2.5	36.5	45.1	43.4	11.4	0.1	4.2	10.3
523	4.1	25.5	45.6	43.1	11.2	0.1	3.5	9.9
523	6.5	17.4	46.5	42.6	10.8	0.1	3.0	10.0
523	9.7	9.4	47.8	41.7	10.4	0.1	4.1	11.0
523	15.0	6.7	47.4	41.6	10.9	0.1	2.1	9.6
523	19.2	4.9	47.7	41.7	10.5	0.1	1.8	9.8
CoAl-1173								
493	2.5	15.1	55.3	38.6	6.0	0.1	1.5	9.5
503	2.5	29.6	50.7	42.2	7.0	0.1	0.7	10.1
513	2.5	51.3	45.8	45.3	8.6	0.3	0.7	6.2
523	1.7	86.2	39.8	47.7	12.4	0.2	tr	1.6
523	2.5	67.2	41.7	46.6	11.5	0.2	tr	5.9
523	4.1	48.3	44.0	45.3	10.6	0.1	tr	7.1
523	6.5	37.1	44.9	44.7	10.3	0.1	tr	7.2
523	9.7	29.1	45.3	44.3	10.2	0.2	tr	7.0
523	15.0	20.4	45.8	44.0	10.1	0.1	tr	6.4

[a] Liquid hourly space velocity (cc/h/g catalyst).
[b] Conversion is given for octenes, octanone, dioctylethers and other products.
[c] Selectivity is equal to the amount of product formed divided by total octanol converted.

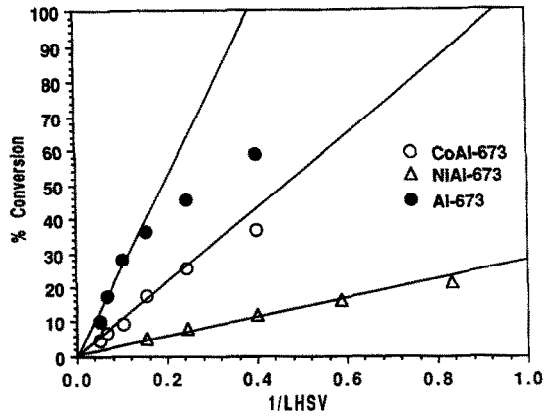

Fig. 6. Effect of liquid hour space velocity (LHSV) on 2-octanol conversion over (●) alumina, (○) cobalt–alumina and (△) nickel–alumina catalysts calcined at 673 K.

kcal/mol for the dehydration of 2-propanol over alumina catalysts. Pines and Manassen [25] reported activation energy values ranging from 19 to 38 kcal/mol for the conversion of various secondary and tertiary alcohols over alumina catalysts. The activation energies (Table 7) for the dehydrogenation of 2-octanol over nickel–alumina catalysts vary from about 9 to 16 kcal/mol and are comparable to the value (18.4 kcal/mol) reported by Davis and Ganesan [22] for the dehydrogenation of 2-octanol over zirconia.

Comparison of the selectivity for dehydration products (S_{III+IV}) is shown in Fig. 9 for alumina, nickel–alumina and cobalt–alumina catalysts at a reaction temperature of 523 K as a function of 1/LHSV. The selectivity for dehydration is close to 100% for alumina, and for cobalt–alumina it is 95% or greater for calcination at 673 or 1173 K. However, the nickel–alumina catalyst calcined at 673 K exhibited about 60% selectivity for dehydration products; and this increases to about 78% when this material is calcined at 1173 K. As expected, the selectivity for octene production parallels closely the dehydration selectivity.

The 1-octene selectivity as a function of 1/LHSV is shown in Fig. 10 for alumina,

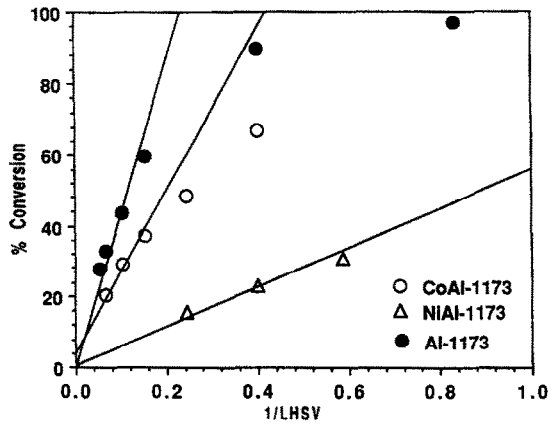

Fig. 7. Effect of liquid hour space velocity (LHSV) on 2-octanol conversion over (●) alumina, (○) cobalt–alumina and (△) nickel–alumina catalysts calcined at 1173 K.

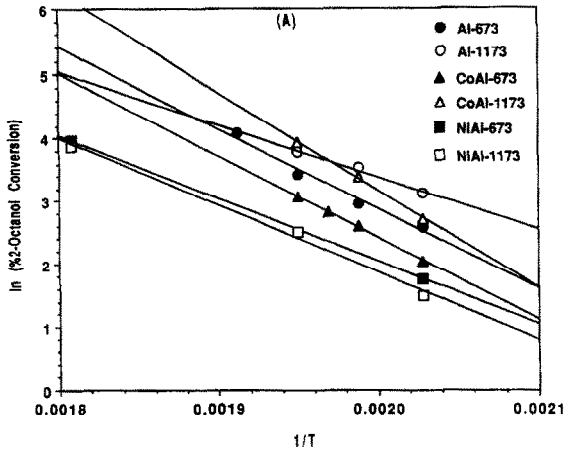

Fig. 8. Effect of reaction temperature on the activity of alumina and nickel–alumina coprecipitated catalysts for 2-octanol reaction. (●, ○) Alumina catalysts calcined at 673 and 1173 K, respectively; (▲, △) cobalt–alumina calcined at 673 and 1173 K, respectively; (■, □) nickel–alumina catalysts calcined at 673 and 1173 K, respectively.

Table 7
Activation energy values (E_a) for the conversion of 2-octanol over alumina, cobalt–alumina and nickel–alumina catalysts

Catalyst	Activation energy (E_a) (kcal/mol)			
	total conversion	dehydration	ethers	dehydrogenation
Al-673	19.1	19.1	12.5	—
Al-1173	16.5	16.8	10.3	—
CoAl-673	25.9	26.4	25.3	—
CoAl-1173	30.6	30.8	20.0	—
NiAl-673	19.9	27.4	18.6	8.8
NiAl-1173	20.6	22.7	21.0	16.2

cobalt–alumina and nickel–alumina catalysts calcined at 673 and 1173 K. The selectivity of 1-octene falls in the range of 38 to 48% for all the three catalysts for these two calcination temperatures. The selectivity for 1-octene decreases with increasing reaction temperature (Tables 3–6) for the three catalysts.

Alumina and cobalt–alumina produce very little, if any, dehydrogenation of 2-octanol. The selectivity for dehydrogenation for the nickel–alumina calcined at 673 K is about 40% and this selectivity decreases to about 22% as the calcination temperature of nickel–alumina catalyst increases to 1173 K. It is likely that the dehydrogenation activity is due, in part or completely, to the presence of Ni oxide impurities. The dehydrogenation selectivity of cobalt–alumina catalyst decreases from about 4% to almost zero as the calcination temperature increases to 1173 K.

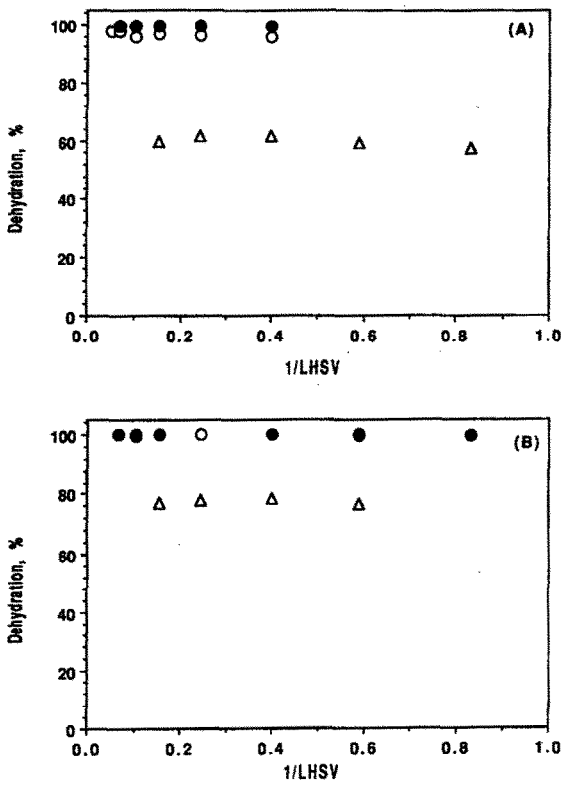

Fig. 9. Comparison of dehydration selectivities for (●) alumina, (△) nickel–alumina and (○) cobalt–alumina catalysts calcined at 673 K (A) and 1173 K (B) as a function of 1/LHSV.

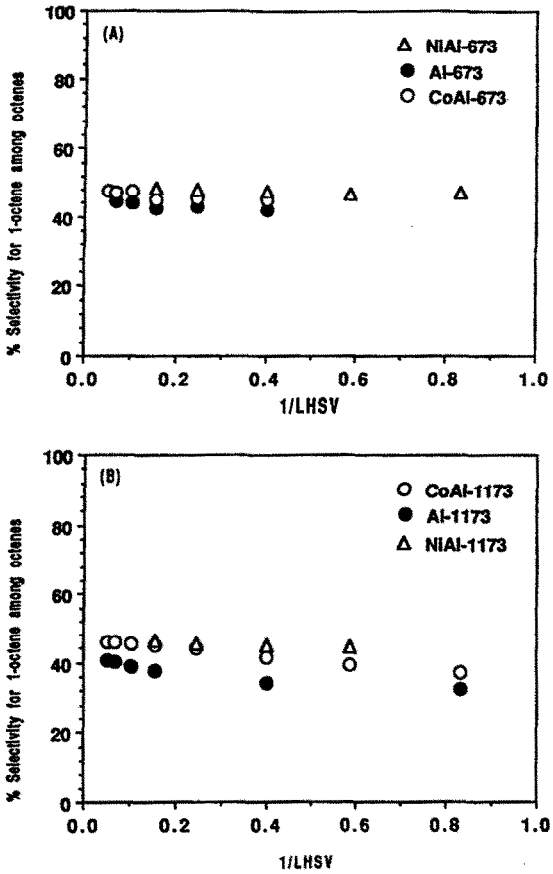

Fig. 10. 1-octene selectivity for (●) alumina, (△) nickel–alumina and (○) cobalt–alumina catalysts calcined at 673 K (A) and 1173 K (B) as a function of 1/LHSV.

4. Conclusions

The introduction of cobalt or nickel into alumina may lead to different types of materials such as the formation of spinel compound or segregation of oxide phase or a mixture depending on the experimental conditions. The crystallinity of the spinel depends on the calcination temperature and increases with the increase of calcination temperature.

The results for 2-octanol conversion suggest that nickel–alumina coprecipitated catalysts have both dehydration and dehydrogenation activity. The dehydrogenation selectivity de-

creases, and the dehydration selectivity increases, with calcination temperature of the catalyst precursor. The activity of the cobalt–alumina catalysts is greater than that of the nickel–alumina catalysts.

The octene distributions (1-octene, *cis*- and *trans*-2-octene) are essentially the same for alumina, nickel–alumina and cobalt–alumina catalysts at a reaction temperature of 523 K. The selectivity for 1-octene decreases with reaction temperature for the catalysts. The major difference among the catalyst series is lower activity and dehydration selectivity for the nickel–alumina catalysts compared to alumina and cobalt–alumina catalysts. The differences are more pronounced at lower reaction and lower calcination temperatures. The present data show that both the inverse ($NiAl_2O_4$) and normal ($CoAl_2O_4$) spinel compounds are active for 2-octanol conversion and that both resemble alumina. Thus, it appears that Al^{3+} in either tetrahedral or octahedral sites exhibit similar sites for 2-octanol conversion and this leads to similar product selectivities as well as showing that the alumina catalyst sites are not altered by the substitution of Co or Ni ions.

References

[1] G. Busca, V. Lorenzelli, V.S. Escribano and R. Guidetti, J. Catal. 131 (1991) 167.
[2] K. Mocala and A. Navrotski, J. Am. Chem. Soc. 72 (1989) 826.
[3] L.W. Bruggraf, D.E. Leyden, R.L. Chin and D.M. Hercules, J. Catal. 78 (1992) 360.
[4] G. Busca, V. Lorenzelli and V.S. Escribano, Chem. Mater. 4 (1992) 595.
[5] B.R. Stromeir and D.M. Hercules, J. Phys. Chem. 88 (1984) 4922.
[6] O. Clause, B. Rebours, E. Merlen, F. Trifiro and A. Vaccart, J. Catal. 133 (1992) 231.
[7] I.A.P.S. Murthy and C.S. Swamy, Catal. Lett. 27 (1994) 103.
[8] A. Navrotsky and O.J. Kleppa, J. Inorg. Nucl. Chem. 29 (1967) 2701.
[9] P. Arnoldy and J.A. Mouljin, J. Catal. 93 (1985) 1335.
[10] S. Brunauer, P.H. Emmet and E. Teller, J. Am. Chem. Soc. 60 (1938) 409.
[11] J.C.P. Broekhoff and J.H. deBoer, J. Catal. 9 (1967) 15.
[12] A.M. Gadalla and T.W. Livingston, Thermochim. Acta 145 (1989) 1.
[13] R.L. Chin and D.M. Hercules, J. Phys. Chem. 86 (1982) 360.
[14] H.G.J. Lansink Rotgerink, H. Bosch, J.G. Van Omen and J.R.H. Ross, Appl. Catal. 27 (1986) 41.
[15] V.D. Allred, S.R. Buxton and J.P. McBridge, J. Phys. Chem. 61 (1957) 117.
[16] W.S. Brey, Jr. and B.H. Davis, J. Collid. Interface Sci. 70 (1979) 10.
[17] M. Lojacono, J.L. Verbeek and G.C.A. Schuit, J. Catal. 29 (1973) 463.
[18] B.H. Davis and W.S. Brey, Jr., J. Catal. 25 (1972) 81.
[19] B.H. Davis, J. Org. Chem. 37 (1972) 1240.
[20] B.H. Davis, S. Cook and R.W. Naylor, J. Org. Chem. 44 (1979) 2142.
[21] J.H. deBoer, R.B. Fahim, B.G. Linsen, W.J. Visseren and W.F.N.M. de Vleesschauwer, J. Catal. 7 (1967) 163.
[22] B.H. Davis and P. Ganesan, I&EC Prod. Res. Dev. 18 (1979) 191.
[23] B.H. Davis, J. Catal. 52 (1978) 176.
[24] C.R. Narayanan, S. Srinivasan, A.K. Datye, R. Gorte and A. Biaglow, J. Catal. 138 (1992) 659.
[25] H. Pines and J. Manassen, Adv. Catal. 16 (1966) 49